Evolution of the Pt Layer Deposited on MgO(001) by Pulsed Laser Deposition as a Function of the Deposition Parameters: A Scanning Tunneling Microscopy and Energy Dispersive X-ray Diffractometry/Reflectometry Study

Guido Scavia,*,† Elisabetta Agostinelli,† Sara Laureti,† Gaspare Varvaro,† Barbara Paci,‡ Amanda Generosi,‡ Valerio Rossi Albertini,‡ Saulius Kaciulis,§ and Alessio Mezzi§

Area di Ricerca ROMA 1, Istituto di Struttura della Materia, CNR, via Salaria km 29.500, 00016 Monterotondo Scalo, Roma, Italy, Area di Ricerca di Tor Vergata, Istituto di Struttura della Materia, CNR, Via del Fosso del Cavaliere 100, 00133 Roma, Italy, and Area di Ricerca ROMA 1, Istituto per lo Studio di Materiali Nanostrutturati, CNR, via Salaria km 29.500, 00016 Monterotondo Scalo, Roma, Italy

Received: September 26, 2005; In Final Form: January 24, 2006

A combined ultrahigh vacuum scanning tunneling microscopy (STM-UHV) and energy dispersive X-ray diffractometry/reflectometry (EDXD/EDXR) study of the evolution of face-centered cubic (fcc) Pt layer growth on MgO(100) by pulsed laser deposition as a function of the process parameters such as deposition temperature and deposition duration has been carried out. The aim of this study is to define the best experimental conditions to obtain a controlled film deposition selective on the Pt growth direction (either [111] or [002]). The evolution of the Pt surface morphology as a function of the deposition temperature (T_{dep}) from 300 to 700 °C has been studied with STM and ED techniques. Results show that the Pt surface, characterized at $T_{dep} = 300$ °C by a 3D island morphology, evolves at higher temperatures to a morphology in which the original islands coexist with a distribution of orthogonal 2D stripes. The two features can be associated with the [111] and [002] Pt growth directions of the fcc phase, respectively. For $T_{dep} = 700$ °C, the island morphology of the (111) face completely disappears, while the merging process of the (002) stripes reaches completion. The evolution of the morphology at $T_{dep} = 600$ °C as a function of the deposition time and thickness has then been studied with STM-UHV, revealing an initial growth of mosaic-like 3D islands. These independent islands, already interconnected, expand along two orthogonal directions and, for longer deposition times, lead to the texture of orthogonal stripes. The EDXR characterization providing the morphological parameters of the films, i.e., thickness and roughness, confirms the above observation and quantifies the effect of such morphological changes on the surface roughness of the Pt film, an important parameter for applications of Pt films as underlayer in magnetic recording media.

1. Introduction

A big effort has been recently devoted to the study of nanosized magnetic materials with large magnetic anisotropy, such as the L1$_0$ ordered alloys, since such systems can be used in important technological applications such as high-density magnetic recording.[1,2] The nanomagnets can be produced either artificially by nanolithographic techniques or directly deposited as nanogranular films. In the case of a direct preparation of the nanostructured film, the final morphology of the layer is fundamental in determining the magnetic properties, in particular the coercivity, which is strongly influenced by microstructural properties.[3,4] It is still under debate whether the isolated island morphology of the layer is beneficial in obtaining films with higher coercivity and also what is the value of critical thickness for obtaining a continuous layer for each specific system. As an example, some authors have recently demonstrated[5,6] the growth by sputtering of FePt/MgO(001) films with very high anisotropy deposited as disconnected islands, that is, with a thickness below the minimum value needed for reaching

continuity, which was estimated to be approximately 50 nm. On the other hand, other authors have reported, for the same system, a decrease of coercivity on passing from the continuous to the separated islands structure and located the critical thickness close to 4.2 nm.[7] Similar systems, such as CoPt face-centered trigonal (001) oriented films, are also widely studied for high-density magnetic recording.[8] They are usually deposited on MgO(001) with a platinum underlayer. During the growth, the Pt underlayer morphology has to be rigorously controlled, to determine in a reproducible way the microstructure of the magnetic layer whose properties are strongly influenced by the underlayer.[9] In particular, the growth of a discontinuous or continuous film should be in principle induced by a templating Pt underlayer with a 3D separated island or a layer-by-layer morphology, respectively. As far as the Pt underlayer is concerned, platinum grows heteroepitaxially on MgO(100), even if they are dissimilar materials with a large mismatch (approximately 6.84%). Typical of metallic films grown on nonwetting oxidic substrates such as MgO is the formation of networks of irregularly shaped nuclei. It is well-known that the crystallographic orientation of epitaxial platinum films depends on various deposition parameters such as growth temperature, pressure (in particular oxygen pressure[10]), and film thickness. Different process conditions are reported in the literature,

---

* Corresponding author. E-mail: guido.scavia@ism.cnr.it.
† Area di Ricerca ROMA 1, Istituto di Struttura della Materia.
‡ Area di Ricerca di Tor Vergata, Istituto di Struttura della Materia.
§ Area di Ricerca ROMA 1, Istituto per lo Studio di Materiali Nanostrutturati.

depending on the deposition method used.[10-15] Pt films grown by techniques such as e-beam evaporation often consists of a mixture of [111] and [001] orientations, while films grown by a plasma with a significant nonthermal contribution [sputtering or pulsed laser deposition (PLD)] can be brought more easily to the formation of a single-oriented layer. This work is hence dedicated to the study of the growth of Pt layers deposited on MgO(100) by PLD. The final goal is to optimize the PLD deposition process in order to obtain, in a reproducible and controlled process, the desired structural and morphological properties in view of its application as underlayer. The study has been performed by varying the parameters that influence the PLD depositions and film growth, i.e., substrate temperature, Pt layer thickness, and postdeposition annealing treatments in the first stages of growth, where major changes of the structural and morphological properties are expected. A microstructural study with STM-UHV and ED-XRD will be presented. Chemical composition of the films has been studied by using X-ray photoelectron spectroscopy (XPS) combined with Ar ion sputtering. The discussion of the results is organized into three sections. In the first section, the effect of the deposition temperature is shown: four temperatures have been chosen in order to cover all the stability range of the most important Pt layer orientations, i.e., from 300 to 700 °C. In the second section, the evolution of the layer morphology as a function of the layer thickness at $T_{dep} = 600$ °C deposition temperature and the effect of postannealing treatments onto some of the corresponding layers are presented. The growth temperature of 600 °C has been chosen because a mixed morphology can still be obtained at this temperature, and one or the other growth directions can be favored by varying other growth parameters. Finally, the experimental results are discussed.

2. Experimental Section

A pulsed KrF excimer laser with 248-nm wavelength was used to deposit Pt layers on polished MgO single-crystal substrates cut and polished along the (100) plane. Substrate and target (a disk of platinum metal) were assembled in a frontal geometry at 5.6-cm reciprocal distance in a high-vacuum chamber. The commercial magnesium oxide substrates and the Pt targets were cleaned in ultrasonic baths with acetone and 2-propanol at boiling point. In the final step, the clean surface was washed with fresh demineralized water with a residual resistivity of 18.2 MΩ cm for some minutes. To ensure thermal contact with the heating element, the substrates were glued with silver paste onto the substrate holder, which was made of a copper pellet heated by a halogen lamp. The Ag paste never came in contact with the growing film, and even at the highest deposition temperature no contamination due to Ag traces was found in the Pt film. A K-type thermocouple was mounted inside the copper pellet at a close distance (1 mm) from the sample. The substrate inside the vacuum chamber was then heated to 400 °C in a vacuum for 6 h and then it was cooled, heated to the final deposition temperature, and stabilized before the beginning of the deposition. Depositions were performed at an energy fluence of 3 J/cm^2 and pulse repetition rate of 10 Hz for a variable number of total pulses (from 1500 to 18000). The variation of energy fluence was accomplished by varying the laser energy while the spot area on the target was kept constant to avoid spurious effect on the deposition rate due to the variation of the irradiated area. Samples were deposited at temperatures ranging from 25 to 700 °C and at a growth pressure of 2×10^{-7} mbar. The background pressure before deposition was close to 8×10^{-8} mbar. This procedure ensured that the

deposited film did not contain impurities, as confirmed by the XPS analysis. The surface characterization has been carried out with a commercial STM-UHV system (WA tech) (typical tunneling parameters: tip−sample voltage = 2−3 V, tunneling current = 0.05−0.08 nA). The STM measurements have been carried out ex situ by transferring the film in the microscope, where the surface was let to degas for at least 12 h before start measuring. All of the analyzed samples were characterized by a conductive Pt layer, even for the thinner cases in which the interconnected Pt islands already form a percolative path for the current. The joint use of diffraction and reflection of X-rays allowed determining the films properties both on the microscopic and mesoscopic scales. Indeed, while the X-ray diffraction provides information on the crystalline structure of the sample, the X-ray reflectometry accounts for its overall morphology in terms of average thickness and surface roughness (variance from the main average thickness). To do this, the energy dispersive (ED) method was used. In the present work, the combined use of the STM and the EDXD/EDXR techniques allowed us to correlate the structural properties of the samples to their morphological characteristics. The main advantages of the ED technique, with respect to the usual angular dispersive one, fully discussed in ref. 16, are connected to the fixed geometry of the experimental apparatus during the measurement. Indeed, in a X-ray scattering experiment, the intensity of the radiation collected at the detector is a function of the scattering parameter q, depending both on the deflection angle and on the energy of the X-ray beam used for the measurement ($q = aE \sin \vartheta$, $a = 1.014$ Å^{-1}/keV). In the energy dispersive variant of the diffractometry/reflectometry techniques, a nonmonochromatized primary beam (in the present case from a W anode X-ray tube) is used, and after the interaction with the sample, the X-ray beam is analyzed by a solid-state detector (SSD), capable of performing the energy scan of the diffracted photons.[16,17] The energy resolution is ca. 1.5% with a maximum count rate of 10 kcounts/s. To reach the desired diffraction (or reflection) angle, source and detector arms are moved by two linear actuators driven by step motors, leading to a minimum scattering angle increment of 0.002°. The experimental setup described above was used to perform both the EDXD and the EDXR measurements, only changing the instrumental configurations, i.e., the order of magnitude of the deflection angle during the data acquisition (10^{-2} Å for reflection and a few Å for diffraction). The first measurements (EDXD) provided the diffraction patterns of the films under study, allowing the investigation of the structural properties. Furthermore, as required for a polycrystalline sample, rocking curve (RC) analyses were performed in order to obtain the statistical distribution of the orientation of the films domains, i.e., their degree of epitaxy. Such analyses were carried out by recording for each film the intensity of the diffracted radiation as a function of an asymmetry parameter [$\alpha = (\vartheta_i - \vartheta_f)/2$], where ϑ_i and ϑ_f are the initial (incidence) and final (deflection) angles and $\vartheta_i + \vartheta_f = 2\vartheta$ is kept constant.[18] The second set of measurements (EDXR) provided the films morphological parameters: thickness and roughness. The fit of the EDXR experimental data was performed using the Parrat's model.[19] Photoemission spectra were collected by using a VG ESCALAB MkII spectrometer, equipped with a standard Al Kα excitation source and a five-channeltron detection system. The experiments were performed at a pressure of about 1×10^{-9} mbar, which was increased up to 1×10^{-7} mbar during the depth profiling. The energy of the ion gun (Ar$^+$) was set to 2.0 keV and the sample current density to 2×10^{-3} mA cm^{-2}, which corresponds to the average sputtering rate of about 0.3

Pt Layer Deposited on MgO(001) by PLD

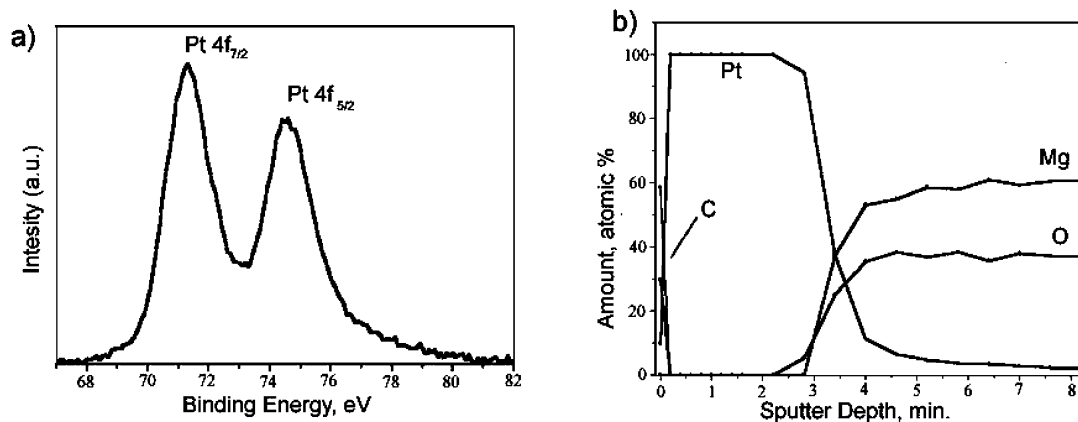*J. Phys. Chem. B, Vol. 110, No. 11, 2006* **5531**

Figure 1. (a) Pt 4f spectrum after the subtraction of Shirley background: Pt $4f_{7/2}$ − BE = 71.1 eV; Pt $4f_{5/2}$ − BE = 74.4 eV. (b) XPS depth profile of the sample grown at the fluence of 3 J/cm^2.
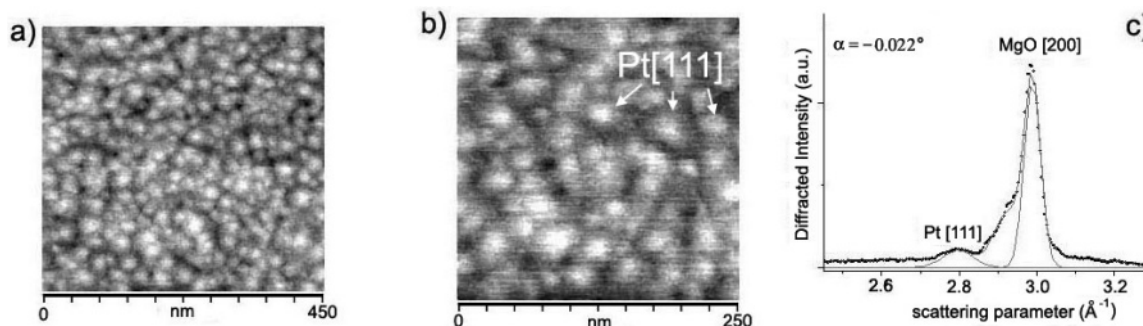

Figure 2. (a, b) STM images of the Pt surface morphology for T_{dep} = 300 °C. (c) EDXD pattern in the q-range of interest. In part b, the correspondence between the typical structures and EDXD peaks is shown by the arrows as examples.

nm min^{-1}. The binding energy (BE) scale was calibrated by measuring the peaks of Au $4f_{7/2}$ (BE = 84.0 eV) from the Au foil mask and C 1s (BE = 285.0 eV) from the surface contamination. The accuracy of the measured BE was ±0.1 eV. More experimental details have been published elsewhere.[20] Depth profiling measurements have been used for the determination of the layers' thickness. The curve thickness/deposition time has been constructed from XPS depth profiles (results not shown here). We verified that, for the deposition times higher than 5 min, the thickness was increasing linearly with time.

3. Results and Discussion

3.1. XPS Characterization. The chemical composition of the sample surface has been investigated by using the XPS technique. In Figure 1a, a typical spectrum of Pt 4f, composed of spin−orbit doublet $4f_{7/2}$ and $4f_{5/2}$ with a separation in energy of 3.3 eV, is shown. The main peak of Pt $4f_{7/2}$ is centered at BE = 71.1 eV, which corresponds[21,22] to metallic platinum. In particular, the XPS depth profiling has been employed to investigate the quality of Pt surface and interfaces. The sample charging effect, which was observed at the interface with insulating substrate, has been eliminated from the depth profile by shifting the main XPS peaks. As can be seen from Figure 1b, the carbon contaminants, which were present only on the surface of the samples exposed to air, are removed quickly, after about 10 s of sputtering. The depth profiling demonstrates that the Pt layer is metallic and that the surface of MgO substrate is clean.

3.2. Pt Layer Morphology as a Function of the Temperature. STM images of Figures 2−5 show the evolution of the surface morphology at four different deposition temperatures, i.e., 300, 500, 600, 700 °C, respectively, for a fluence of 3 J/cm^2

and deposition times of 15 min (thickness of 8 nm). The results must be compared with the EDXD structural characterization (in Figures 2−5) and the EDXR morphological characterization (Figures 6 and 7). The structural characterization showed the presence of the face-centered cubic (fcc) Pt phase at every deposition temperature. The main difference as a function of T was the amount of crystalline domains grown along the [001] and the [111] direction, respectively, to evaluate the epitaxy degree around such directions. Actually, in this case, only the second-order reflection [002] is visible. This information is obtained by performing the RC analyses of the films by EDXD (as discussed in paragraph 2), and it consists of a sequence of diffraction patterns collected by progressively increasing the asymmetry parameter. An example is shown in Figure 8 for the sample deposited at 600 °C. To make the comparison with the STM images, a representative single pattern is shown for each sample in Figures 2−5. For T_{dep} = 300 °C, according to the STM images of Figure 2a, b, the layer is characterized by a homogeneous distribution of small 3D islands with a mean diameter of 11 nm and roughness of 1.2 nm. From a comparison between STM and EDXD (Figure 2, parts b and c, respectively), these 3D islands, which represent the only features visible in the STM analysis of the layer at 300 °C, can be attributed to the [111] Pt observed by EDXD. Beside the MgO contribution, the [111] Pt is the only reflection present in the patterns. For T_{dep} = 500 °C, the Pt layer is characterized by two distinct 3D features (Figure 3a): a mesh of orthogonal short stripes that form a regular network and the 3D islands of Figure 2, now more expanded and with an hexagonal base, which fills the empty spaces inside the mesh network. Enlarged images (inset of Figure 3a) reveal that each island is composed by a stacking of several layers whose area decreases by moving from the
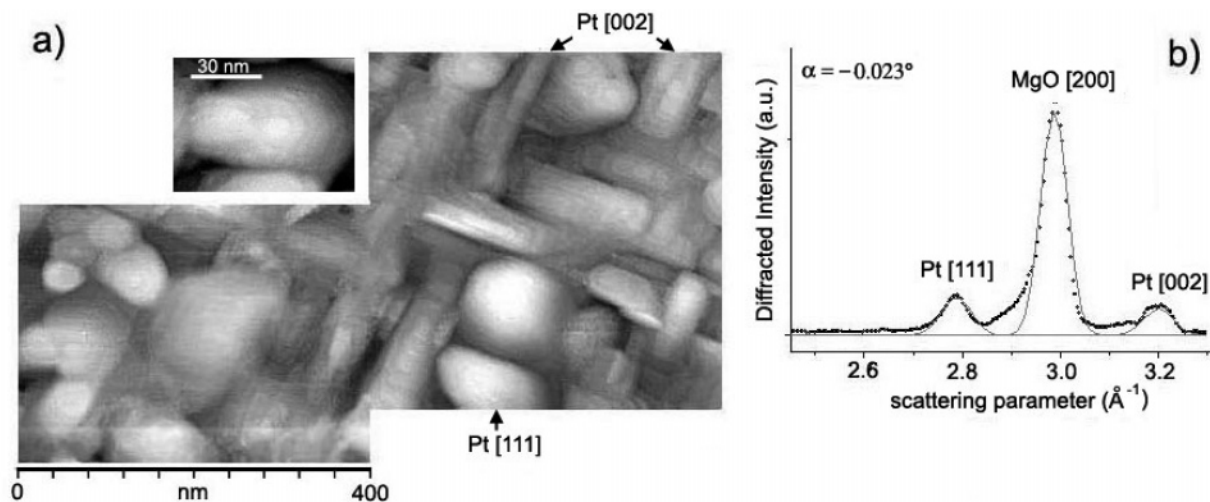
Figure 3. (a) STM image of the Pt surface for $T_{dep} = 500$ °C. (b) EDXD pattern in the q-range of interest. In part a, the correspondence between morphological features and EDXD peaks is shown by the arrows; in the insert, a magnification of one [111] Pt island is shown.
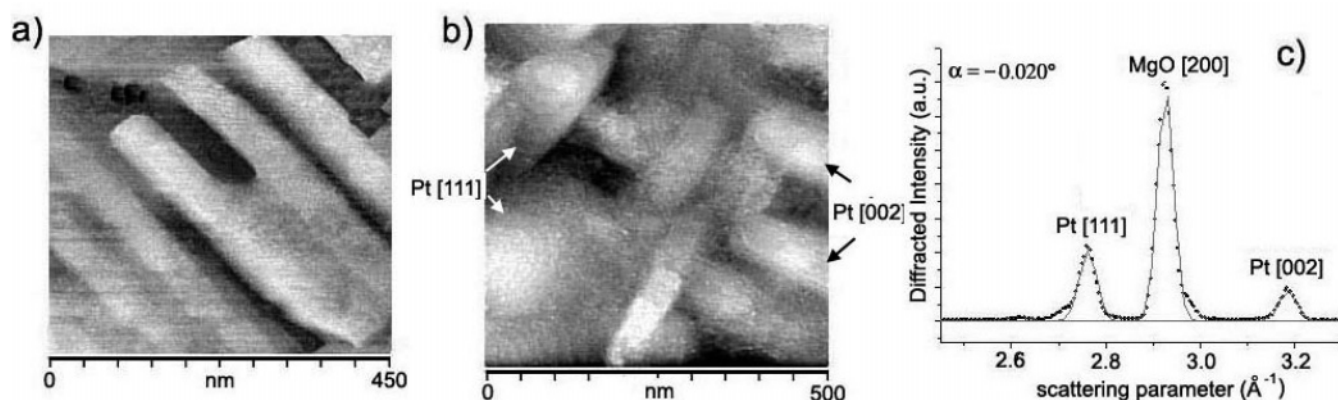

Figure 4. (a, b) STM image of the Pt surface for $T_{dep} = 600$ °C. (c) EDXD pattern in the q-range of interest. The correspondence between morphological features of part b and EDXD peaks is shown by the arrows.
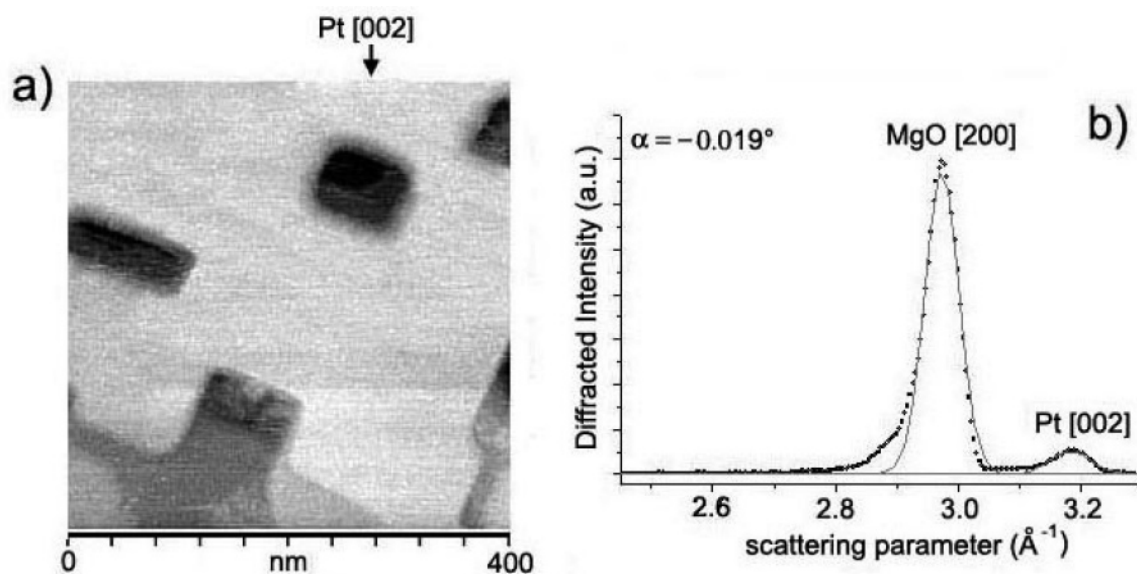

Figure 5. (a) STM image of the Pt surface for $T_{dep} = 700$ °C. (b) EDXD pattern in the q-range of interest. The correspondence between morphological structures of part a and EDXD peaks is shown by the arrow.

substrate to the film surface. Also the stripes show this pyramidal structure, but the staking layers are in this case elongated rectangles rather than hexagons. The 3D growth observed at the lowest temperatures can be explained by the Pt kinetic energy not being high enough to allow a long-range Pt migration

and, subsequently, a layer-by-layer growth. A diffraction pattern of the sample for $T_{dep} = 500$ °C is reported in Figure 3b. The [111] Pt reflection is still present but, in addition, the [002] Pt reflection is also visible, showing the coexistence of the two growth orientations. From a comparison with Figure 3a, the
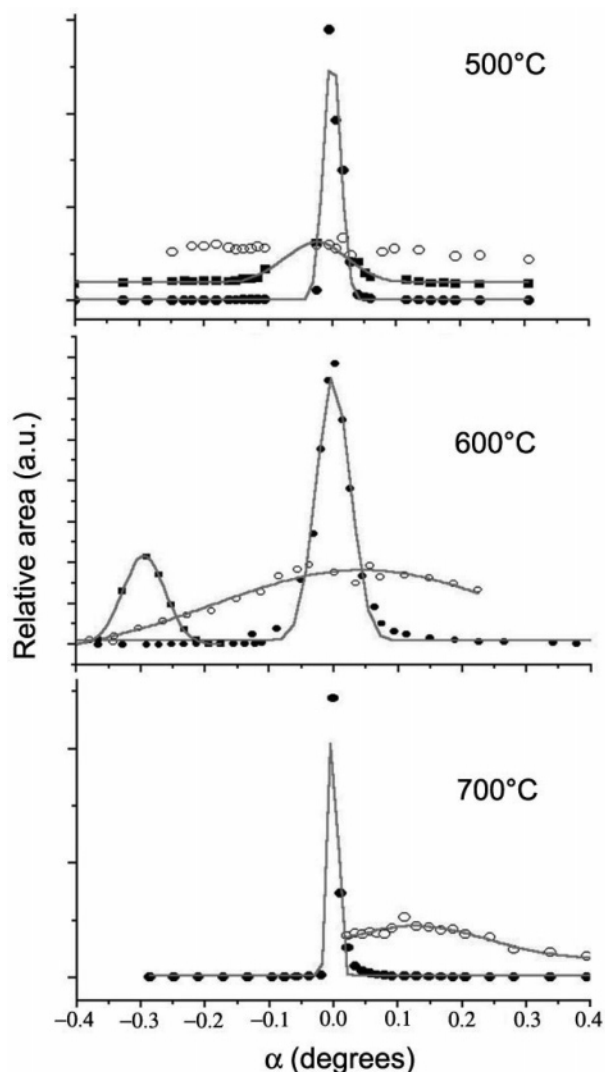
Pt Layer Deposited on MgO(001) by PLD

J. Phys. Chem. B, Vol. 110, No. 11, 2006 **5533**

Figure 6. Results of the RC analysis: empty dot, [002] Pt; full dot, [200] MgO; full square, [111] Pt.
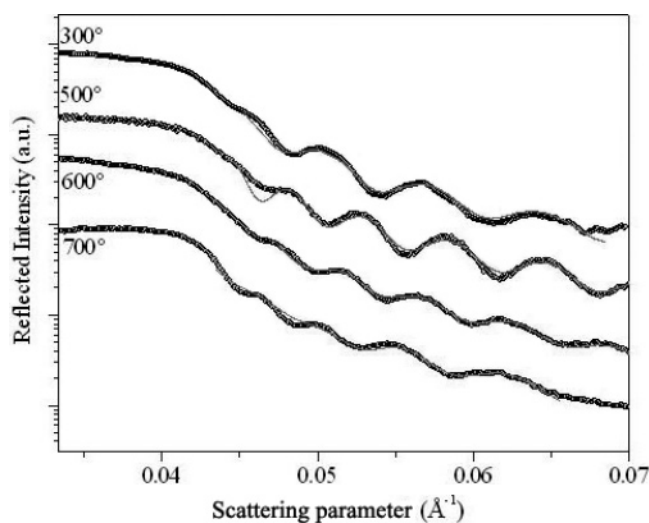

Figure 7. EDXR patterns: experimental data and fits.

presence of the pyramidal islands observed by STM, which can be considered an evolution of the smaller islands at 300 °C, has to be associated with the [111] Pt reflection. As far as the [002] Pt reflection is concerned, since the presence of this peak corresponds to the appearance of the stripe mesh structure, a

correspondence between the peak and the stripes can be hypothesized, as evidenced in Figure 3a. By increasing the deposition temperature to 600 °C (Figure 4a,b), the stripes appear larger and better defined, as compared to the 500 °C case. Besides, within each stripe, the upper surfaces are bidimensional and composed by one single flat layer. According to Figure 4b, the mesh structure is dominant with respect to the hexagonal islands which, even if present, have a very low density. The forklike shape (Figure 4a) suggests that a merging process between adjacent stripes starts occurring. The two reflections are still both present in EDXD patterns (Figure 4c). Finally, for T_{dep} = 700 °C, the coalescence between the expanding stripes has actually led to flat epitaxial terraces due to the higher annealing temperature (Figure 5a). The edges of the terraces are in prevalence orthogonal, thus reproducing and maintaining the orthogonality of the original stripes attributable to the [002] Pt. As a matter of fact, according to the EDXD data, only the [002] Pt reflections are present in the patterns recorded for this sample (see Figure 5b). On the other hand, a distribution of squared holes all over the terrace can be observed (see Figure 5a). The holes have a depth of several layers and they can be explained as the result of a nonperfect coalescence of the various stripes, i.e., the areas left empty by the expanding stripes. The same kind of holes are present in the annealed samples, as will be shown later. This suggests that such imperfect coalescence for the 700 °C case is induced by an annealing effect during the deposition. A detailed inspection of the sample surface excludes the presence of residual 3D hexagonal islands, and this is confirmed by the absence of [111] Pt reflection. The result of the RC analysis on the samples deposited at the various temperatures (Figure 6) is the following: (1) the [111] Pt orientation shows in all cases a considerable degree of epitaxy (fwhm < 0.1°). (2) The maxima of the RC of the Pt film do not coincide with the reference value (α = 0°), at which the substrate reflections from the substrate are most intense but slightly displaced. This can be explained, either to the effect related to a possible miscut of the substrate, and to a slight variation of the film orientation with respect to the substrate, depending on the lattice match between Pt and the MgO. The thickness of the films deduced by EDXR is not correlated with the widths (fwhm) of the respective RC, which indicates that the substrate/film misorientation is small and random and it can be attributed to the statistical process of deposition. (3) Concerning [002] Pt at 500 °C (Figure 6), the corresponding RC is rather flat (very large growth orientation distribution) while at 600 °C it is broad but peaked. This can be interpreted as a higher degree of order of the [002] Pt growth direction at this temperature and is consistent with the improved regularity in the sequence of the stripe structure observed by STM. For the sample deposited at 700 °C, a higher degree of epitaxy was observed [fwhm = 0.270(5)°], even thought the texture of [002] crystallites does not reach the epitaxy observed for the [111] oriented crystallites. The results of the EDXR investigation, reported in Figure 7, allowed us to estimate both the film thickness and the roughness. The sequence of the EDXD patterns at 600 °C as a function of the α scan degree is reported in Figure 8. The roughness as a function of the deposition temperature is shown in Figure 9. It is interesting to note that, on passing from the 3D to the 2D regime, the roughness unexpectedly increases. However, this can be easily attributed to the presence of the holes and, in general, of the empty spaces amidst the flat stripes. In other terms, the stripes at 600 °C and terraces at 700 °C show very flat top surfaces, but being separated by deep canyons, the thickness variations
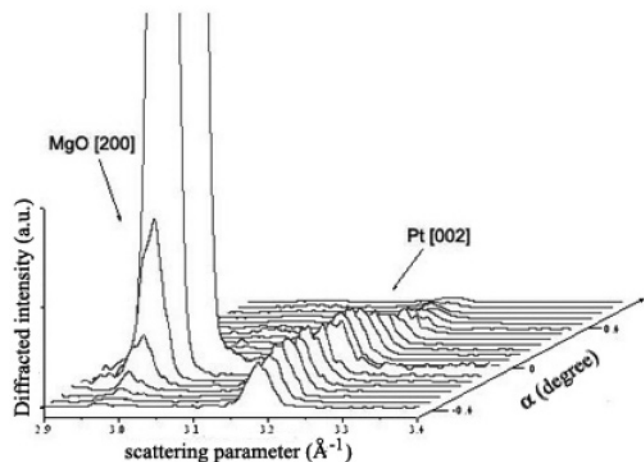
Figure 8. Sequence of the EDXD patterns (in the *q*-range of interest) for the sample deposited at 600 °C acquired during the α scan (RC). The observable reflections are [200] MgO at $q = 2.982(4)$ Å^{-1} and [002] Pt at $q = 3.187(4)$ Å^{-1}.
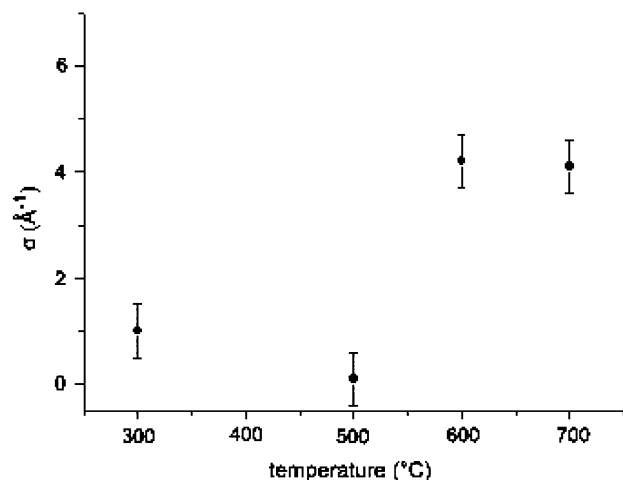

Figure 9. Roughness as a function of the deposition temperature.

dominate and the roughness has an high value. Conversely, samples deposited in the 300−500 °C T range are more homogeneous, and although do not exhibit flat structures, nevertheless, they have an overall lower roughness.

3.3. Pt Layer Morphology as a Function of the Layer Thickness. Figure 10 shows the surface evolution as a function of the Pt layer thickness in a set of different films deposited at 3 J/cm^2 at $T_{dep} = 600$ °C for a variable thickness, and each was separately measured in the STM. For a deposition time (t_{dep}) of 2.5 min (thickness value (d) of 1.5 nm) (Figure 10a), the surface is characterized by a distribution of independent, highly packed, interconnected islands that even at this stage guarantee the electrical conductance needed for STM measurements. The islands have a mean diameter of 20 nm, if each island is approximated to a circle and a mean height corresponding to the layer thickness. As a matter of fact, the islands have a noncircular shape, and the corresponding edges are straight lines oriented along two orthogonal preferential directions. Each island can expand along one of the two directions or along both the directions simultaneously, thus generating small segments or L-shaped structures, respectively. These islands tend to form a flat pavement, and the roughness can be mainly attributed to the empty spaces left between adjacent islands, as discussed above. By moving to $t_{dep} = 3.5$ min ($d = 1.8$ nm) (Figure 10b), the islands expand by establishing more interconnections. In

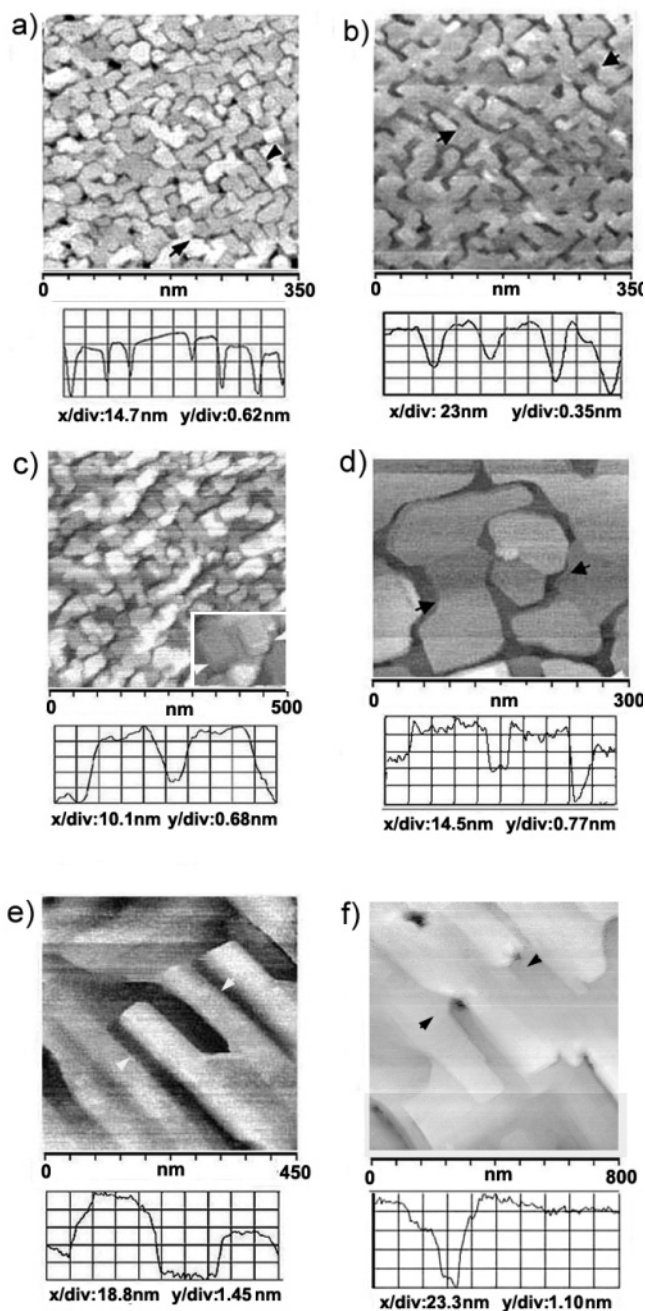**Figure 10.** Pt surface morphology after deposition at $T_{dep} = 600$ °C, fluence 3 J/cm^2 for deposition times of (a) 2.5 min (thickness (d) = 1.5 nm), (b) 3.5 min ($d = 1.8$ nm), (c) 5 min ($d = 2.5$ nm) (in the inset, a detail is shown), (d) 7 min ($d = 4.5$ nm), (e) 15 min ($d = 9$ nm), and (f) 25 min ($d = 15$ nm). The corresponding profiles along the lines delimited by the arrows are shown.

this process, each island becomes more irregular and richer in elbows, thus acquiring a mosaic-like shape, although the two orthogonal preferential growth directions are maintained. Due to the coalescence, both the typical length and the width of each island increases. On passing from $t_{dep} = 2.5$ to 3.5 min (from $d = 1.5$ to 1.8 nm) the island height does not sensibly change, thus suggesting that, after a first stage in which the islands are subjected to a 3D growth, by moving to longer deposition times, the lateral expansion prevails over vertical growth. At $t_{dep} = 7$ min ($d = 4.2$ nm) (Figure 10d), the coalescence of the islands leads to flat terraces of the same height and delimited by straight lines. It is interesting to note that the height of the terraces even at $d = 4.2$ nm does not sensibly change with respect to the
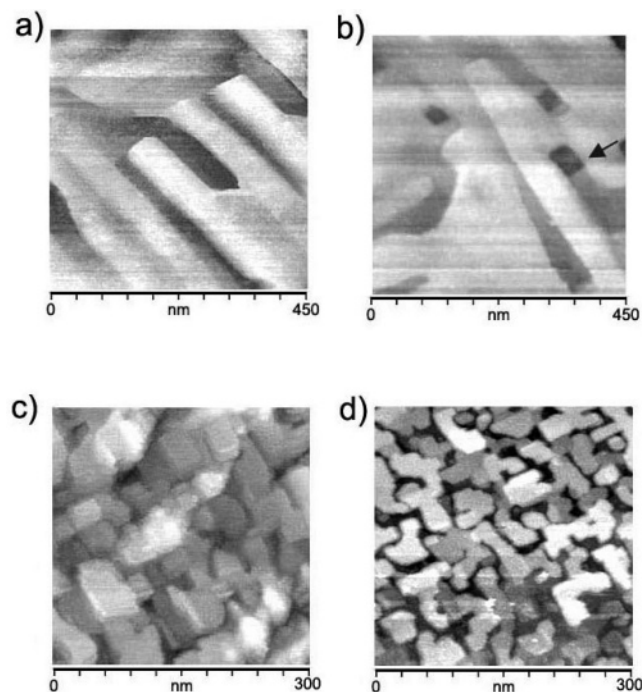
Pt Layer Deposited on MgO(001) by PLD

J. Phys. Chem. B, Vol. 110, No. 11, 2006 **5535**

Figure 11. Effect of the flash annealing at 300 °C onto the surface morphology for the cases at T_{dep} = 600 °C, fluence = 3 J/cm² for deposition times of 15 min (a, b) and 5 min (c, d) and a thickness of 9 nm (a, b) and 2.5 nm (c, d). The surfaces before annealing are shown in a, c and after are shown in b, d.

height of the islands of the previous cases. By moving to t_{dep} = 10 min (d = 6 nm) (results not shown here) and then to 15 min (d = 9 nm) (Figure 10e), the surface is characterized by a sequence of long stripelike layers oriented along the two orthogonal directions, thus forming a mesh structure. Furthermore, the stripe width increases with deposition time. According to Figure 10e, the roughness within each stripe is very low (<1 nm), although the average roughness exceeds 1.5 nm, due to the steep sequence of the narrow flat terraces and empty spaces, as anticipated at the end of section 3.2. Finally, the surface morphology after a massive deposition of Pt, for t_{dep} = 25 min (d = 15 nm), is shown in Figure 10f. The layer reaches the minimum roughness attributed to the presence of a 2D sequence of terraces onto the surface. Besides, the layer, even almost continuous, is characterized by a homogeneous distribution of holes due to an imperfect filling of the underlying terraces. These holes, however, tend to become smaller and smaller by further increasing the thickness (results not shown here). In summary, the layer passes from a 3D morphology, consisting of interconnected islands, to a 2D morphology, characterized by the stripe mesh. The two orthogonal directions along which the 3D mosaic-like islands expand are maintained in the relative orientation of the stripes in the mesh structure, thus suggesting that the former network represents a sort of precursor unit of the latter structure. The fact that after a certain deposition time the morphology evolves from small islands into long stripes can be attributed both to a higher Pt atoms density onto the surface and to a permanence for longer times at high temperature, i.e., to an annealing effect.

Finally, a study on the effect of annealing onto the surface morphology was carried out on some of the previous samples. The annealing was performed by flash Joule heating at temperatures ranging between 300 and 350 °C under UHV conditions within the STM. Figure 11 shows the surface morphology before and after the UHV annealing treatment for

samples deposited at 600 °C with F = 3 J/cm² for t_{dep} = 15 min (d = 9 nm) (a, b) and 5 min (d = 2.5 nm) (c, d). For the 15 min (d = 9 nm) case, in which the Pt layer has completed the total coverage of the substrate, the effect of the annealing is to favor coalescence and enlargement of the stripes. Consequently, the formation of larger flat terraces is observed, as shown in Figure 11b. According to the roughness profiles, although the height of the terraces did not sensibly change in these cases, the width of the terrace has increased; within a single terrace, a surface roughness of approximately 5 Å was estimated. It can be hypothesized that the short annealing induced a redistribution of the Pt atoms onto the surface, thus causing the broadening of the terraces without major structural changes. For a longer annealing time, surface degradation started to occur, due to some Pt clusterization onto the surface (results not shown here). Another effect of the annealing is to favor the formation of holes with rectangular shape. These holes form almost independently on the thickness and they are likely to be a consequence of the atomic redistribution. If a continuous layer is required, the hole formation represents a shortcoming of the annealing process. Figure 11c,d shows the effect of the annealing before and after the flash annealing for the layer with a thickness of 2.5 nm deposited for 5 min, i.e., for the case in which interconnected islands are present. After the annealing, the spaces between the mosaic-like islands increase, unlike the previous case, although a percolation still occurs and the islands form continuous paths. The annealing of films at low coverage stages seems then to increase the separation between islands.

4. Conclusions

A study on the morphology of Pt layers grown on MgO-(001) by pulsed laser deposition as a function of the deposition temperature and deposition time has been carried out with a combined use of STM-UHV and EDXD/EDXR.

Results show that the temperature has a significant role in determining the layer morphology. For T_{dep} = 300 °C, a 3D island distribution characterizes the Pt layer. This morphology can be assigned to the fcc [111] Pt crystalline growth direction observed by EDXD. At T_{dep} = 500 °C, the coexistence of two 3D features, i.e., a homogeneous network of orthogonal stripes and hexagonal islands between, associated with the [002] Pt and to the [111] Pt respectively, occurs. For T_{dep} = 600 °C, the two features and the two corresponding EDXD reflections are still present. Moreover, the stripes show flatter top surfaces and form a more ordered network. Finally, for T_{dep} = 700 °C, the stripe coalescence produces flat terraces that can be associated with the only residual [002] Pt growth direction, and the unique element of discontinuity is represented by regularly shaped holes.

The 3D morphology observed at relatively low temperature can be attributed to the kinetic energy of Pt atoms not being high enough to allow a long-range migration and consequently a rearrangement of Pt atoms. The impinging atoms prefer to grow vertically onto the already formed 3D islands rather than expanding laterally. At higher temperature the kinetic energy allows this migration and the 3D structure turns into a 2D pattern.

For T_{dep} = 600 °C, a STM analysis of the surface as a function of the deposition time reveals the initial formation of a 3D layer composed by regularly shaped mosaic-like islands. By increasing the thickness, these islands expand laterally and then coalesce, thus forming an almost continuous pavement onto which a layer-by-layer growth occurs. This 2D growth consists of the formation of a sequence of orthogonal flat terraces. For higher

deposition times, the terrace length increases, thus covering almost all the empty spaces corresponding to the uncovered areas. The evolution from the initial 3D island structure to the 2D orthogonal stripe structure can be attributed to the longer annealing effect and to a higher Pt atom density on the surface.

The effect of the UHV annealing is to produce a broadening of the terraces in the 2D growth regime and an increase of the interisland separation channels in the 3D regime. However, a general collateral effect of the annealing is to produce also a distribution of regularly shaped holes.

The results show that the combined use of the STM-UHV and EDXD/EDXR techniques provides the morphological and structural information needed to individuate the appropriate deposition conditions for an oriented film growth, as required for magnetic recording application.

Moreover, the experimental evidences so obtained demonstrate that PLD, although representing a nonequilibrium technique, is able to give epitaxial layers, thanks to the high mobility of the atoms onto the growing surface, also favored by the high substrate temperature.

Further investigations on the role of the MgO (001) substrate in influencing the layer morphology are in progress.

References and Notes

(1) Yanigisawa, M.; Shiota, N.; Yamaguchi, H.; Suganuma Y. *IEEE Trans. Magn.* **1983**, *19*, 1638.

(2) Coffey, K. R.; Parker, M. A.; Howard, J. K. *IEEE Trans. Magn.* **1995**, *31*, 2737.

(3) Ristau, R. A.; Barmak, K.; Lewis, L. H.; Coffey, K. R.; Howard, J. K. *J. Appl. Phys.* **1999**, *86*, 4527.

(4) Ersen, O.; Parasote, V.; Pierron-Bohnes, V.; Cadeville, M. C.; Ulhac-Bouillet, C. *J. Appl. Phys.* **2003**, *93*, 2987.

(5) Shima, T.; Takanashi, K.; Takahashi, Y. K.; Hono, K. *Appl. Phys. Lett.* **2002**, *81*, 1050.

(6) Takanashi, K.; Shima, T.; Takahashi, Y. K.; Hono, K.; Li, G. Q.; Ishio, S. Joint European Magnetic Symposia, Dresden, Germany, Sept 5−10, 2004; p 174.

(7) Wan, J.; Huang, Y. H.; Skumryev, V.; Stoyanov, S.; Zhang, Y.; Hadjipanayis, G. C.; Weller, D. Joint European Magnetic Symposia, Dresden, Germany, Sept 5−10, 2004; p 173.

(8) Cebollada, A.; Farrow, R. F. C.; Toney, M. F. *In Magnetic Nanostructures*; Nalwa, H. S., Ed.; 2002; p 93.

(9) Lambeth, D. N. In *Magnetic Storage Systems beyond 2000*; Hadjipanayis, G. C., Ed.; Nato Science Series, II, Mathematics, Physics and Chemistry, 41; Kluwer Academic Plublishers: Norwell, MA, 2001; p 55.

(10) Takai, Y.; Sato, M. *Supercond. Sci. Technol.* **1999**, *12*, 486.

(11) McIntyre, P. C.; Maggiore, C. J.; Nastasi, M. *J. Appl. Phys.* **1995**, *77*, 6201.

(12) McIntyre, P. C.; Maggiore, C. J.; Nastasi, M. *Acta Mater.* **1997**, *45*, 869.

(13) McIntyre, P. C.; Maggiore, C. J.; Nastasi, M. *Acta Mater.* **1997**, *45*, 879.

(14) Narayan, J.; Tiwari, P.; Jagannadham, K.; Holland, O. W. *Appl. Phys. Lett.* **1994**, *64*, 2093.

(15) Cillessen, J. F. M.; Wolf, R. M.; De Leeuw, D. M. *Thin Solid Film* **1993**, *226*, 53.

(16) Caminiti, R.; Rossi Albertini, V. *Int. Rev. Phys. Chem* **1999**, *18*, 263.

(17) Sinha, S. K.; Sirota, E. B.; Garoff, S.; Stanley, H. B. *Phys. Rev. B* **1988**, *38*, 2297.

(18) Paci, B.; Generosi, A.; Rossi Albertini, V.; Agostinelli, E.; Varvaro, G.; Fiorani, D. *Chem. Mater.* **2004**, *16*, 292.

(19) Parrat, L. G. *Phys. Rev.* **1954**, *95*, 359.

(20) Gaggiotti, G.; Galdikas, A.; Kaciulis, S.; Mattogno, G.; Setkus, A. *J. Appl. Phys.* **1994**, *76*, 4467.

(21) Kaciulis, S.; Mattogno, G.; Galdikas, A.; Mironas, A.; Setkus, A. *J. Vac. Sci. Technol. A* **1996**, *14* (6), 3164.

(22) Moulder, J. F.; Stickle, W. F.; Sobol, P. E.; Bomben, K. D. *In Handbook of X-ray Photoelectron Spectroscopy*; Physical Electronics Inc.: Eden Prairie, MN, 1995.